IS-PORTO 2023 PROCEEDINGS

Proceedings of the 8th International Symposium on DEFORMATION CHARACTERISTICS OF GEOMATERIALS Porto, 3rd - 6th September 2023

Using shear modulus to predict the bearing capacity of strip foundations on sand

Ruan Andrew Murison[1,#] and *Gerhard* Heymann[1]

[1]*University of Pretoria, Department of Civil Engineering, Pretoria, South Africa*
[#]*Corresponding author: ruan.murison@tuks.co.za*

ABSTRACT

This paper reports results of a study to predict load-settlement behaviour of strip foundations on a dry uncemented sand using only soil stiffness data, under both working loads and extreme loads. This involved predicting the strength of a foundation system without using any strength parameters. A non-linear stepwise load-settlement prediction algorithm was utilised, which used the small-strain shear modulus of layers below the footing, a suitable stiffness modulus reduction curve and elasticity theory. The algorithm was adapted to predict the ultimate bearing capacity, as well as to construct a stress-settlement curve and determine the bearing pressure experienced beneath a foundation at any particular settlement. The method was evaluated using two different sets of modulus reduction curves, for small-scale model foundations on loose, medium dense and dense sand. Model tests were conducted at 1g. Particle Image Velocimetry (PIV) was used to observe strains within the soil during loading. These strains were used to calculate the shear modulus of discrete layers throughout loading and back-estimate the layer small-strain shear moduli. Additionally, the mode of shear failure for each test at ultimate bearing capacity was observed using PIV. Modulus reduction curves that initially degrade shear modulus rapidly beyond the elastic threshold strain (0.001%) gave superior predictions under the given conditions. Using such curves, ultimate bearing capacity predictions produced errors of 0.4% to 10.8%. Using the same input parameters, stress-settlement predictions were of satisfactory accuracy over the entire settlement range.

Keywords: shear modulus, shallow foundations, modulus reduction curves, digital image correlation.

1. Background

Terzaghi's approach (Terzaghi 1943) for estimating bearing capacity of shallow foundations has been employed by engineers for many years. Key features of the formulation of the failure mechanism and thus plastic collapse load for drained conditions are the assumption that the internal friction angle is equal to the angle of dilation, and that the soil is perfectly plastic. Although it is known that these are not realistic assumptions, they result in a realistic collapse mechanism (Atkinson 1981).

Two classes of shallow foundation settlement prediction models exist in the geotechnical literature, namely those that incorporate only stiffness parameters, and those that incorporate both strength and stiffness parameters. Recent studies have reported accurate predictions of shallow foundation settlements under working loads, using small-strain shear moduli, modulus degradation data and a non-linear stepwise method (Archer 2014; Archer and Heymann 2015). These techniques, coupled with seismic tests for in-situ small-strain modulus, have proven to predict settlements of full-scale geotechnical structures accurately (Heymann et al. 2017). This study extends the aforementioned stiffness-based predictions beyond serviceable loads to ultimate bearing capacity, without incorporating any strength parameters.

Vesić (1973) established a link between shallow foundation failure mode and the relative density of sands (and thus implicitly the modulus of sands). Fig. 1 shows the influence of relative density and embedment depth on the mode of foundation shear failure. The objective of this study was to evaluate the accuracy of the prediction algorithm for load-settlement behaviour under serviceable and extreme loads, for model foundations on each of loose, medium dense and dense sand.

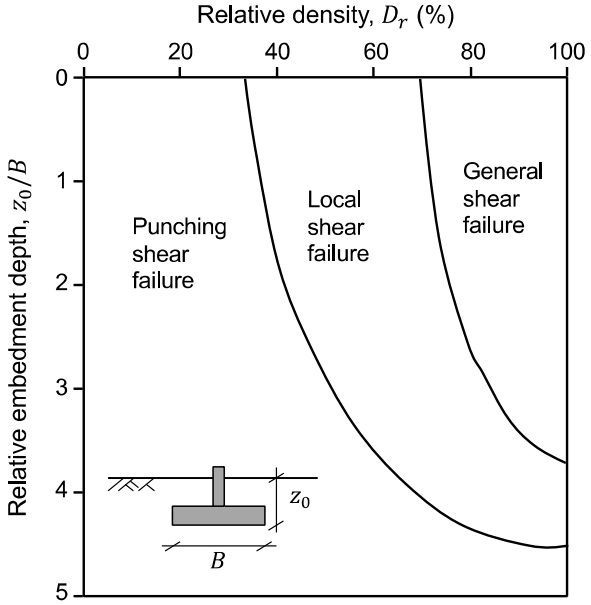

Figure 1. Influence of relative density on shear failure mode (after Vesić 1973).

2. Experimental setup

The soil used in the laboratory physical models was a dry, uncemented fine silica sand called Cullinan sand. The particle size distribution of Cullinan sand is given in Fig. 2, and properties of the sand are given in Table 1. A 150 × 82.5 × 30 mm rigid aluminium model strip footing was used. Sandpaper was glued to the bottom of the footing to simulate a rough soil-footing interface.

Models were prepared to relative densities of 12% (loose), 48% (medium dense) and 90% (dense) in a centrifuge strongbox with a clear glass window. The loose model was carefully placed by hand with no further compaction. The medium dense model was air-pluviated from a constant drop height. The dense model was dry tamped in 8 layers of equal mass and height.

Plane strain conditions were modelled by facilitating contact between the footing and the front and back boundaries. The boundary effects due to friction on these interfaces were considered to be negligible. The footing was placed on the ground surface and loaded under deflection control using a hydraulic jack powered by an electric motor. The load ram force and displacement were measured using a load cell and linear variable differential transformer (LVDT) fixed to the actuator. Footing displacement was assumed to be equal to displacement of the load ram, neglecting any possible bedding errors or deflection of the stiff load frame. The tests were conducted at 1g. The experimental setup of the physical model is illustrated in Fig. 3.

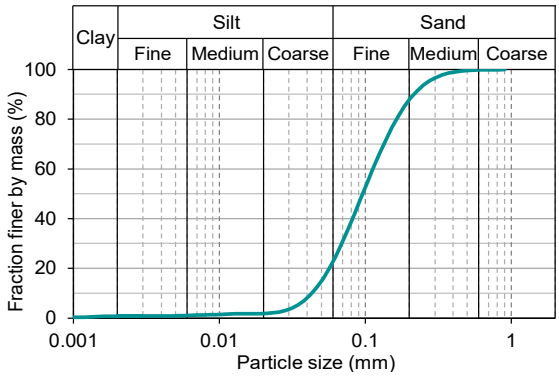

Figure 2. Cullinan sand particle size distribution.

Table 1. Properties of Cullinan sand

Description	Uncemented silica sand		
USCS Classification*	SPu (poorly graded, uniform, slightly silty sand)		
Particle shape	Angular to subrounded		
Specific gravity	2.694		
Min. dry density (kg/m³)*	1379		
Max. dry density (kg/m³)*	1704		
Max. void ratio, e_{max}	0.953		
Min. void ratio, e_{min}	0.576		
Poisson's ratio, ν'	0.3 (assumed for modelling)		
Model	**Loose**	**Medium dense**	**Dense**
Dry density (kg/m³)	1412	1521	1670
Void ratio, e	0.908	0.771	0.613
Relative density, D_r (%)	12.1	48.4	90.2

* Determined according to ASTM D2487, D4254, D4253 respectively

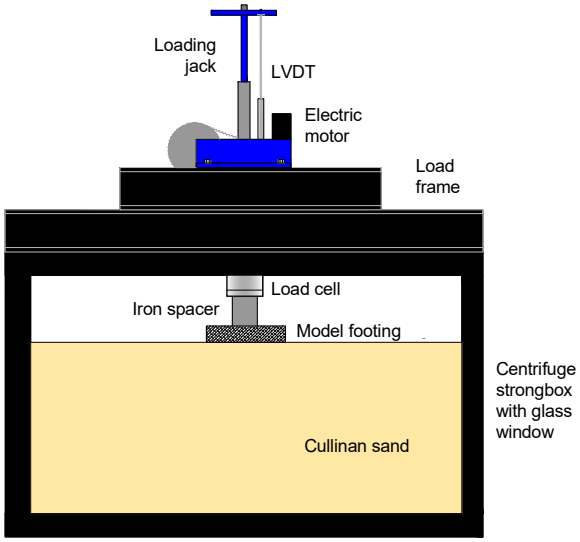

Figure 3. Physical model schematic (not to scale).

3. Modulus degradation

The modulus degradation curves selected for this study take on the form of the hyperbolic modulus reduction curve proposed by Oztoprak and Bolton (2013), given by Eq. (1).

$$\frac{G}{G_0} = \begin{cases} \left[1 + \left(\frac{\gamma - \gamma_e}{\gamma_r}\right)^a\right]^{-1} & \text{for } \gamma > \gamma_e \\ 1 & \text{for } \gamma < \gamma_e \end{cases} \quad (1)$$

where: γ = current shear strain (%)
γ_e = elastic threshold strain (%)
γ_r = reference strain: $G/G_0 = 0.5$ at $\gamma = \gamma_e + \gamma_r$
a = curvature parameter

The gradient of the foundation response depends on the stiffness modulus at any given strain level, thus the bearing stress prediction accuracy at serviceable settlement values is a function of how well the modulus reduction curve describes the stiffness degradation throughout loading. It is noteworthy that although the curve approaches a modulus of zero, it never reaches zero, regardless of the level of strain. For this reason, a settlement-based failure criterion needed to be assumed since the modulus reduction curves do not allow the foundation stress-settlement curve to peak or plateau. Functional foundation failure was assumed to occur at a settlement (s) equal to 10% of the width of the foundation (B), which is a typical assumption (Briaud 2007). This criterion was applied for both the predictions and for the experimental results, if no objective stress peak occurred prior to a relative settlement (s/B) of 0.1.

4. Prediction algorithm

The prediction algorithm used by Archer and Heymann (2015) to predict settlement based on a given bearing pressure was modified to predict the bearing stress for any given level of settlement. The foundation geometry in question for all equations used by the algorithm is displayed in Fig. 4. The proposed non-linear stepwise algorithm that was used for bearing capacity prediction is as follows:

1. Divide the material beneath the foundation into sublayers, based on seismic test results (or another appropriate laboratory or in-situ test). Material to a depth below the footing of at least twice the foundation width should be considered.
2. Assign G_0 to each sublayer, determined from a suitable test. G_0 is related to the small-strain Young's modulus (E_0') through elasticity theory:

$$E_0' = 2G_0(1 + \nu') \quad (2)$$

3. Calculate the vertical stress increase ($\Delta\sigma_{z,i}'$) and horizontal stress increase ($\Delta\sigma_{h,i}'$) at the centre of each sublayer *i,* due to the increase in foundation stress per load step (Δq). A step size of $\Delta q = 0.01$ kPa was used. $\Delta\sigma_{z,i}'$ and $\Delta\sigma_{h,i}'$ are calculated at the centre of the width of the footing using Eqs. (3) and (4), derived from Boussinesq's theory (Boussinesq 1885). The depth to the centre of layer *i* is represented by z_i.

$$\Delta\sigma_{z,i}' = \frac{\Delta q}{\pi}\left\{2\,\mathrm{atan}\left(\frac{B}{2z_i}\right) + \sin\left[2\,\mathrm{atan}\left(\frac{B}{2z_i}\right)\right]\right\} \quad (3)$$

$$\Delta\sigma_{h,i}' = \frac{\Delta q}{\pi}\left\{2\,\mathrm{atan}\left(\frac{B}{2z_i}\right) - \sin\left[2\,\mathrm{atan}\left(\frac{B}{2z_i}\right)\right]\right\} \quad (4)$$

4. Initial vertical strain increment ($\Delta\varepsilon_{z0,i}$) for each sublayer *i* is calculated using the small-strain shear modulus for each layer ($G_{0,i}$). Vertical strain increments can be calculated by Eq. (5), assuming plane strain conditions for an ideal elastic soil.

$$\Delta\varepsilon_z = \frac{1}{2G}\left[(1 - \nu')\,\Delta\sigma_z' - (\nu')\,\Delta\sigma_h'\right] \quad (5)$$

Plane strain shear strain invariant increments ($\Delta\varepsilon_\gamma$) can be calculated by Eq. (6). This is useful when the chosen modulus reduction curve is in terms of shear strain.

$$\Delta\varepsilon_\gamma = \frac{1}{2G}(\Delta\sigma_z' - \Delta\sigma_h') \quad (6)$$

5. For each subsequent load step *j*, the starting strain per sublayer is the sum of all strain increments for that sublayer thus far. The starting strain and a suitable modulus reduction curve are used to determine the new shear modulus per sublayer for load step *j*, G_{ij}. This shear modulus is used in Eq. (5) to calculate the vertical strain increments for load step *j*.
6. Settlement per load step *j* (s_j) is the sum of the product of each layer thickness (H_i) and layer vertical strain increase ($\Delta\varepsilon_{z,i}$): $s_j = \sum_{i=1}^{m} H_i \cdot \Delta\varepsilon_{z,i}$. Total settlement ($s$) is the sum of settlements over all the load steps. Thus for *n* load steps and *m* sublayers:

$$s = \sum_{j=1}^{n}(s_j) = \sum_{j=1}^{n}\sum_{i=1}^{m}(H_i \cdot \Delta\varepsilon_{z,i})_j \quad (7)$$

7. Step 3-6 are repeated for each load increment. When the total settlement is equal to 10% of the footing width, the bearing stress after the subsequent load step is returned as the ultimate bearing capacity (q_f).
8. The load-settlement curve is constructed by plotting total settlement versus applied load at the end of each load increment.

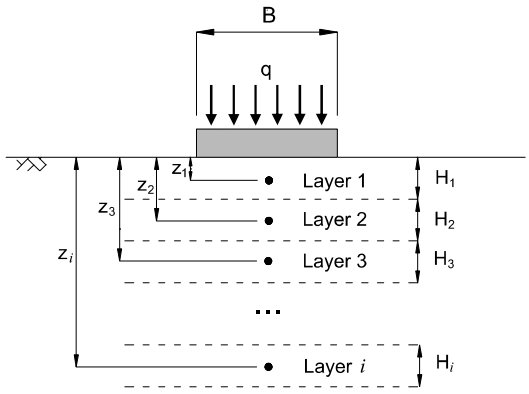

Figure 4. Prediction algorithm geometry and nomenclature.

5. Particle Image Velocimetry

5.1. Shear modulus analysis

Photogrammetric techniques were used to calculate shear strains and thus shear moduli throughout loading. GeoPIV-RG (Stanier et al. 2016) was the programme utilized. Photographs were taken at 5 s intervals and patches of 50 × 50 px, spaced 25 px c/c, were used for all analyses (50 px ≈ 14.8 mm ≈ 0.18B). The model was discretised into six sublayers, each approximately equal to half of the footing width. The GeoSTRAIN_RG function was used to determine the maximum engineering shear strain (γ_{max}) throughout loading, at the centre of each sublayer along the footing centreline. This strain is equivalent to the diameter of the Mohr circle of strain and the plane strain shear strain invariant (ε_γ) per Eq. (8), where ε_1 and ε_3 are the major and minor principal strains respectively. The principal strains are determined graphically for triangular elements by the GeoSTRAIN_RG function.

$$\gamma_{max} = \varepsilon_\gamma = \varepsilon_1 - \varepsilon_3 \quad (8)$$

The surface stress determined from the load cell and Eqs. (3) and (4) were used to determine the principal stresses acting at each sublayer centroid throughout loading. Eq. (9) was subsequently used to calculate the shear modulus (G) for each sublayer at the given shear strain, assuming that the major principal stress is vertical.

$$G = \frac{1}{2\varepsilon_\gamma}(\sigma_z' - \sigma_h') \quad (9)$$

Two reasonable sets of fitting parameters for curves taking on the form of Eq. (1) could be determined for the photogrammetric modulus reduction curves, each set resulting in the back-calculation of the same small-strain modulus. The 'Set 1' parameters describe rapid stiffness degradation beyond the elastic threshold strain, whereas the 'Set 2' parameters facilitate more gradual initial stiffness degradation. The parameters for each test are given in Table 3, and the back-calculated layer small-strain modulus values are given in Table 2. The modulus reduction behaviour and the two fitted Oztoprak and Bolton (2013) curves for each test are plotted in Fig. 5. Coefficient of determination (R^2) ranges are reported for each fit. Each layer's curve is normalised by the back-calculated small-strain shear modulus. The fitted curves, subsequently used for predictions, are given in Fig. 6.

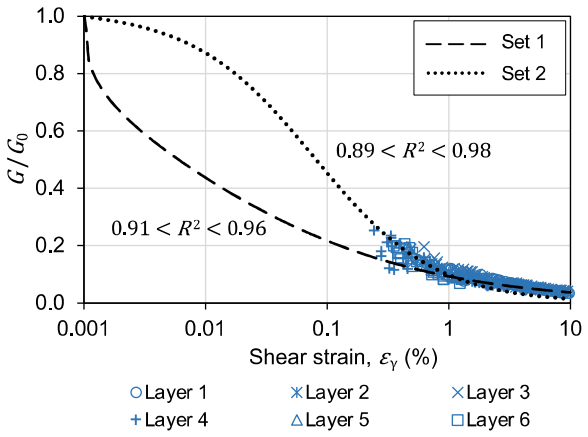

a) Loose test (D_r = 12%)

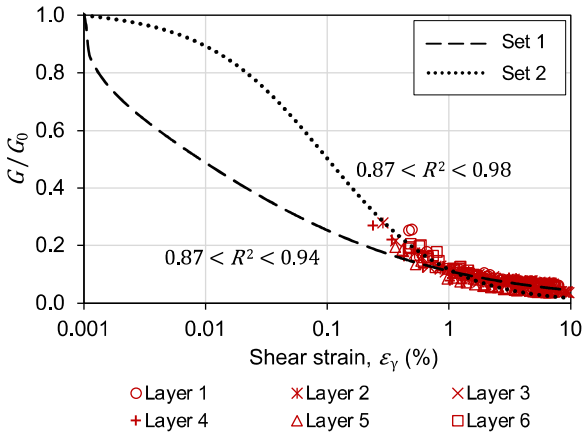

b) Medium dense test (D_r = 48%)

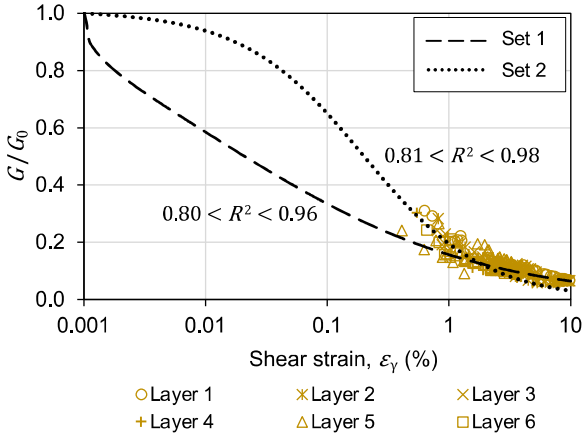

c) Dense test (D_r = 90%)

Figure 5. Layer modulus degradation behaviour determined from PIV.

Table 2. Back-calculated small-strain shear modulus per layer for each test

	G_0 (MPa)		
Layer No.: Depth (mm)	**Loose**	**Medium dense**	**Dense**
Layer 1: 0.0 – 41.3	1.5	4.3	28.1
Layer 2: 41.3 – 82.5	1.5	5.0	30.0
Layer 3: 82.5 – 123.8	1.8	4.3	33.0
Layer 4: 123.8 – 165.0	2.0	4.5	32.9
Layer 5: 165.0 – 206.3	2.1	3.8	24.1
Layer 6: 206.3 – 247.5	2.4	5.6	25.2

Table 3. Oztoprak and Bolton (2013) fitting parameters for two sets of curves fitted through PIV data

Set 1: Rapid initial degradation	**Loose**	**Medium dense**	**Dense**
γ_e (%)	0.001	0.001	0.001
γ_r (%)	0.005	0.008	0.020
a	0.48	0.46	0.44
Set 2: Gradual degradation	**Loose**	**Medium dense**	**Dense**
γ_e (%)	0.001	0.001	0.001
γ_r (%)	0.08	0.10	0.20
a	0.88	0.88	0.88

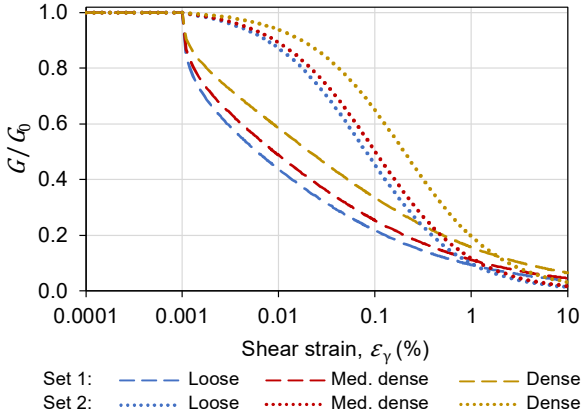

Figure 6. Modulus reduction curves to be used for predictions.

5.2. Full-field analysis: failure mechanisms

PIV analyses were conducted on the full field of each test to determine the mechanism shape and type of failure mode at ultimate bearing capacity. The aim was to determine whether each of the three shear failure modes described in Fig. 1 had been achieved, so that the performance of the prediction method could be evaluated for each. Three typical types of failure mode are depicted in Fig. 7. Displacement vector fields and maximum engineering shear strain fields for each of the tests are given in Fig. 8. No failure planes intersected with model edges and so lateral boundary effects were insignificant.

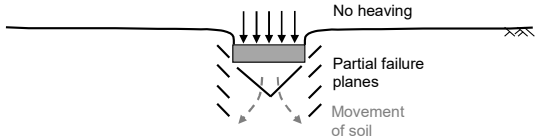

a) Punching shear failure: loose sands

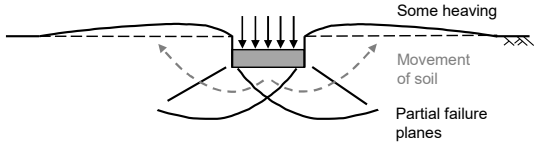

b) Local shear failure: medium dense sands

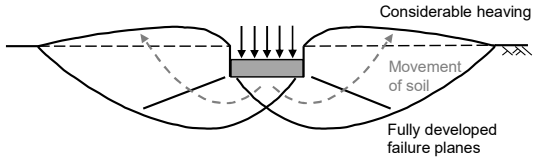

c) General shear failure: dense sands

Figure 7. Typical drained shear failure modes.

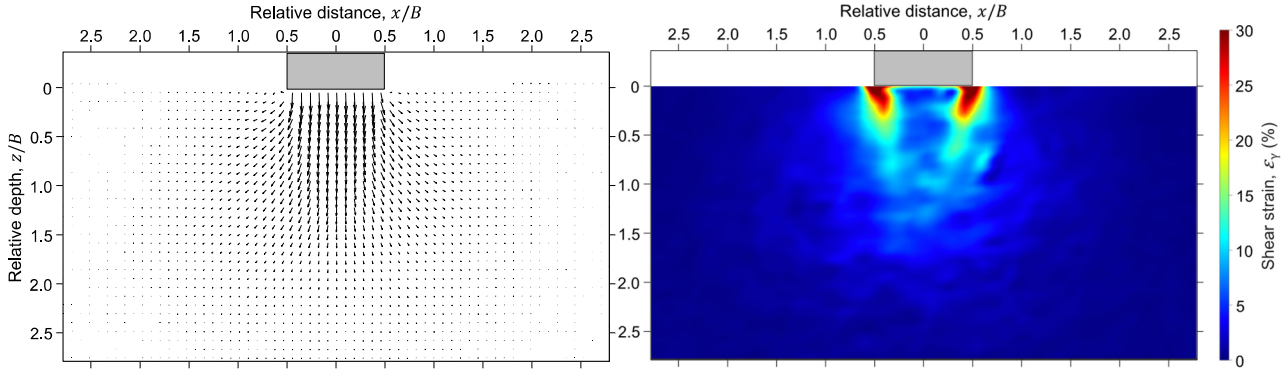

a) Loose test ($D_r = 12\%$): Punching shear failure

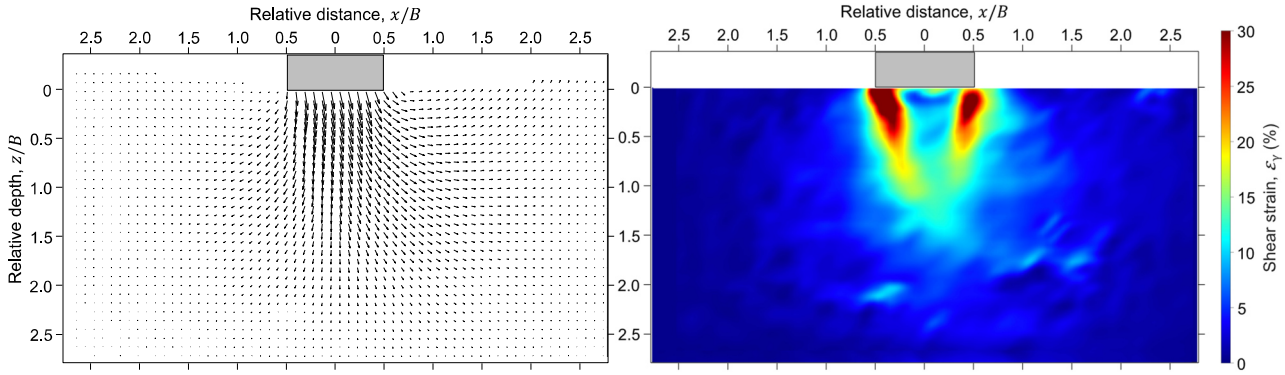

b) Medium dense test ($D_r = 48\%$): Local shear failure

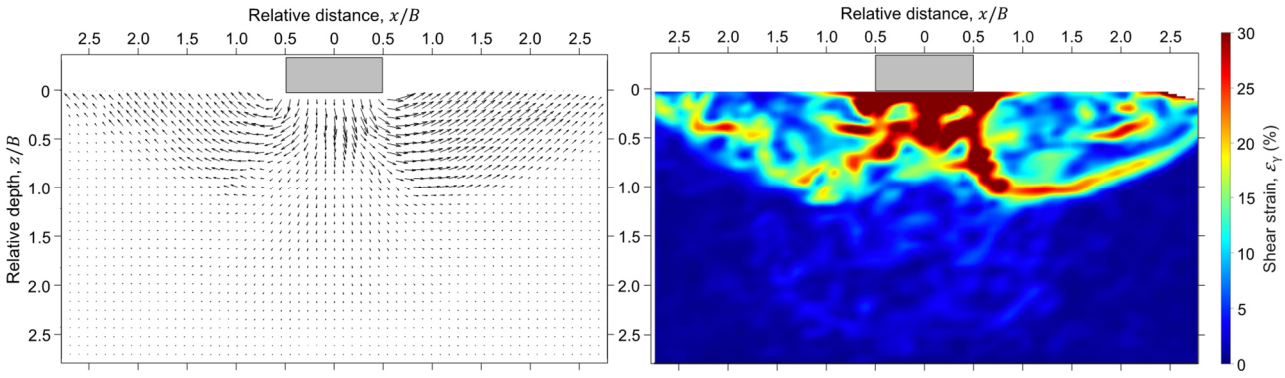

c) Dense test ($D_r = 90\%$): General shear failure

Figure 8. Failure mechanisms illustrated through PIV: displacement vectors (left, vectors scaled up 1.5×) and shear strain (right).

The loose sand test analysis displayed no heaving of the ground surface and stresses were concentrated to the edges of the footing. Displacements were primarily vertical, indicating a compressive mechanism and punching shear failure.

The analysis for the medium dense sand test showed some heaving of the ground surface adjacent to the footing. Displacements were predominantly vertical directly beneath the footing, but lateral displacements were present beyond the edge of the footing. The failure was driven by a combination of compression and shear, and indications of partially formed shear planes suggest that local shear failure had occurred.

The dense sand test analysis showed considerable ground surface heave and brittle failure (plastic collapse). Logarithmic spiral shaped shear planes were fully formed due to strong dilation, and displacements of the slip wedges were lateral and upward, indicating a shear-driven mechanism. These signs suggest that general shear failure had occurred under a mechanism consistent with the well-known slip shape for drained foundation failure.

Each test showed the failure mode expected according to Vesić (1973) and Fig. 1, allowing the suitability of the bearing capacity prediction method to be evaluated for all three modes of shear failure of foundations in dry sand. Additionally, it is noteworthy that the observable displacements occurred within stress bulbs not deeper than $z/B \approx 2.0$-2.5, a depth beyond which displacements were relatively insignificant in all three tests. This observation agrees with the decision taken to consider only material up to a depth of three foundation widths ($z \geq 3B = 247.5$ mm) as the practical zone of influence for the shear modulus analysis in Section 5.1 and subsequent predictions in Section 6.

6. Results and discussion

6.1. Prediction and model test results

The stress-settlement curves observed for the model foundations in each test, along with the predictions carried out using the Set 1 and Set 2 modulus reduction curves, are given in Fig. 9.

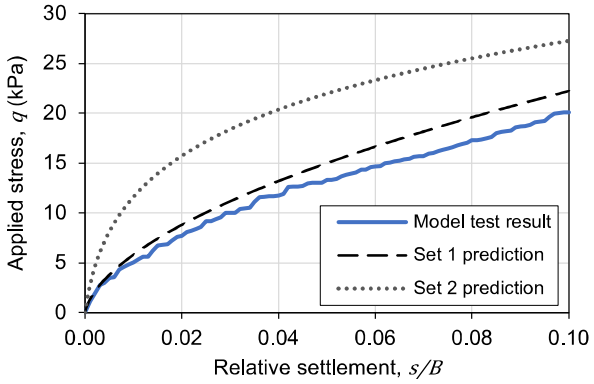

a) Loose test (D_r = 12%)

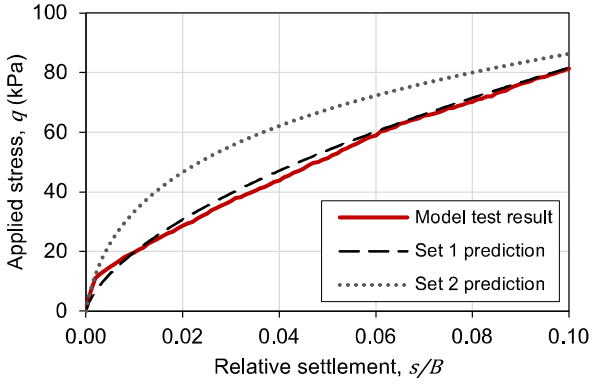

b) Medium dense test (D_r = 48%)

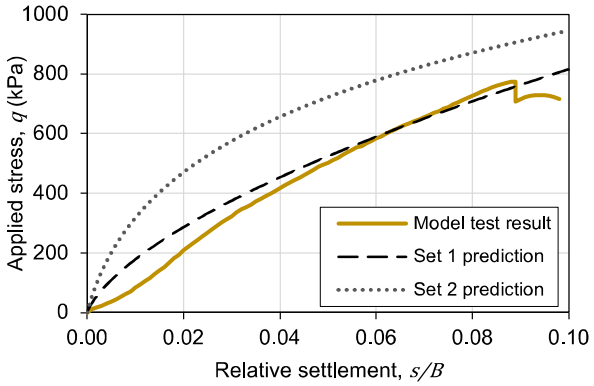

c) Dense test (D_r = 90%)

Figure 9. Model foundation response and nonlinear-stepwise predictions (note different vertical axis scales).

Bearing stress prediction error was defined such that a positive error corresponds with an overprediction, per Eq. (10).

$$\text{Prediction error} = \frac{q_{predicted} - q_{measured}}{q_{measured}} \qquad (10)$$

The predicted and observed ultimate bearing capacity and associated errors for each test and set of modulus reduction curves are given in Table 4.

The standard error (SE) of the prediction error and coefficient of determination (R^2) between predicted and measured stresses were used to evaluate the serviceable bearing stress prediction accuracy over the entire settlement range.

Table 4. Bearing stress prediction results

Test results	**Loose**	**Medium dense**	**Dense**
Bearing capacity, q_f (kPa)	20.07*	81.33*	770.90
s/B at failure	0.10*	0.10*	0.089
* No objective stress peak or plateau			
Set 1 predictions	**Loose**	**Medium dense**	**Dense**
Bearing capacity, q_f (kPa)	22.23	81.65	816.09
q_f Prediction error (%)	10.8	0.4	5.9
R^2 for $s/B \in [0\ ,\ 0.1]$	0.997	0.995	0.981
SE (%) for $s/B \in [0\ ,\ 0.1]$	13.05	8.23	63.74
Set 2 predictions	**Loose**	**Medium dense**	**Dense**
Bearing capacity, q_f (kPa)	27.28	86.31	945.77
q_f Prediction error (%)	35.9	6.1	22.7
R^2 for $s/B \in [0\ ,\ 0.1]$	0.984	0.980	0.962
SE (%) for $s/B \in [0\ ,\ 0.1]$	80.00	39.20	151.08

It was clear that the Set 1 curves, exhibiting rapid initial stiffness degradation, gave superior predictions of stress-settlement behaviour over the entire settlement range as well as at ultimate bearing capacity. The prediction error for Set 1 predictions over the full relative settlement range are given in Fig. 10.

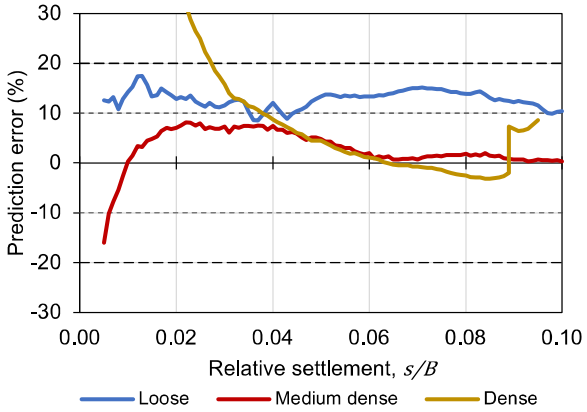

Figure 10. Set 1 prediction errors over full settlement range.

High R^2 values indicate that the shape of the stress-settlement curves were well predicted, which validates the selected fitting parameters for the modulus reduction curves used in the predictions. However, this parameter alone only implies a linear relationship between predicted and measured stresses and is not a sufficient descriptor of prediction accuracy. The standard error of the prediction error is a statistical descriptor of how well the magnitude of stress was predicted over the full range. This depends on both the shape of the input modulus reduction curves, as well as the magnitude of the back-estimated small-strain moduli.

The Set 1 loose test prediction, for example, exhibited a coefficient of determination of nearly 1, but overpredicted the stress across the entire settlement range. This suggests that if the predicted stress-settlement curve were multiplied by some constant, a near-perfect prediction may be achieved. Thus it could be concluded that small-strain modulus values, back-calculated using a softening curve that accurately captures the shape of the foundation response, were greater than the true small-strain moduli of the loose sand strata. This was still considered a satisfactory prediction in the loose test, as the prediction error remained below 20% for all settlements.

The Set 1 medium dense test prediction was the most successful, with a standard error of less than 10% and R^2 of nearly 1. This is a result of modulus reduction curve parameters that accurately describe the shape of the foundation response, as well as realistic back-calculated layer small-strain moduli for the prediction input. The prediction remained within 10% of the test result for all settlements greater than $0.006B$, and the error approached zero as ultimate bearing capacity was reached. It should be noted that for both the loose and medium dense tests, no objective stress peak or plateau was observed, and functional bearing capacity failure was defined at a relative settlement of 0.1. Since this is the same criterion used for the prediction algorithm, bearing capacity prediction depended only on satisfactory prediction of stress-settlement behaviour, and was independent of the assumed failure criterion.

An objective stress peak could be observed for the dense test. Plastic collapse occurred at a relative settlement of 0.089. The relative settlement at failure was sufficiently close to the criterion, resulting in a satisfactory Set 1 ultimate bearing capacity prediction. The prediction algorithm failure criterion of $s/B = 0.1$ was thus deemed suitable. The foundation response prediction at low stresses was largely influenced by bedding errors induced by softening of the dense material when levelling the ground surface prior to testing. This is shown by the stiffening of the test foundation response at approximately $s/B = 0.01$ in Fig. 9c. However, once the effect of bedding errors had been masked at higher stresses, the prediction errors were satisfactorily small. The predicted stress remained within 20% of the model test for $s/B > 0.027$ and within 10% for $s/B > 0.037$.

6.2. A critical state perspective

Whilst a limitation of bearing capacity prediction using Terzaghi's approach is the fact that the mechanism was developed assuming a perfectly plastic soil model, the method proposed in this study assumes nonlinear elastic conditions. Predictions will thus be most accurate when elastic strains are dominant during deformation due to loading. A conceptual elastic-plastic critical state soil mechanics (CSSM) model was considered, where strains remain elastic as long as the yield surface (which is the state boundary surface) is not engaged, and where plastic strains must be generated if the effective stress path (ESP) engages the yield surface. Fig. 11 proposes possible effective stress paths followed during each test, as well as yield curves (i.e. the projections of the intersection of the yield surface and 'elastic walls' upon which strains remain elastic) at yielding and failure. An assumption is that plastic strains were generated upon yielding when any stress path engaged the initial yield curve. Note that initial stress history is denoted by: NC - normally consolidated; LOC - lightly overconsolidated and HOC – heavily overconsolidated.

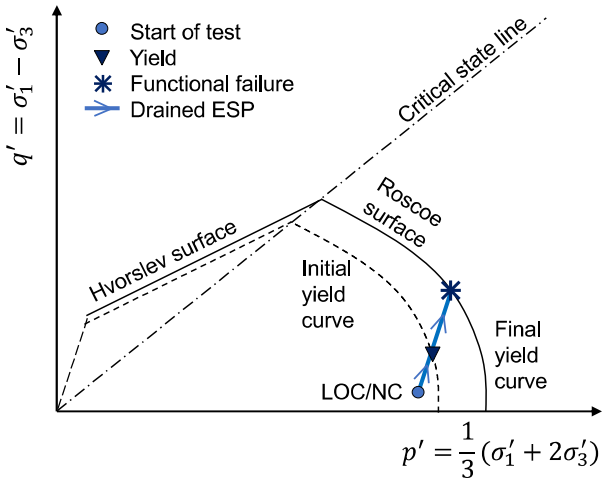

a) Loose test ($D_r = 12\%$)

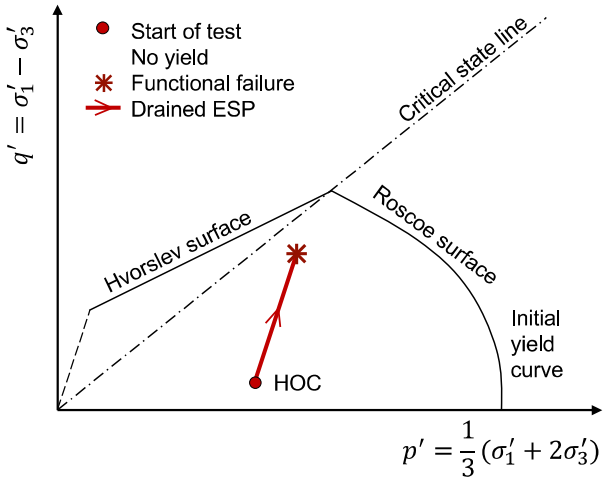

b) Medium dense test ($D_r = 48\%$)

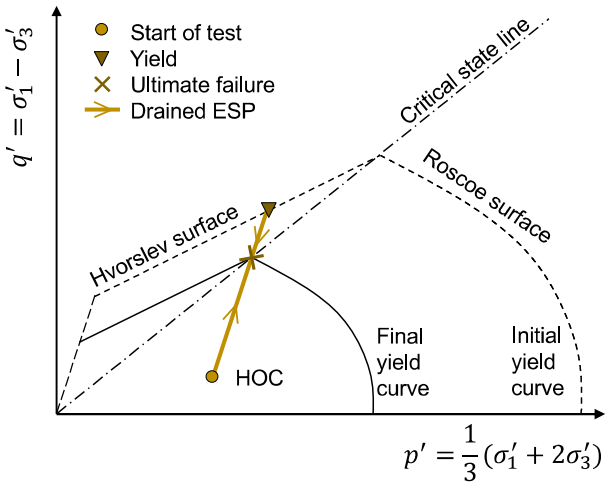

c) Dense test ($D_r = 90\%$)

Figure 11. Hypothesised stress paths.

Considering this CSSM perspective allows for an explanation of the accuracy of each prediction. The loose sand test was placed gently by hand, with the only possible stress history imposed being during moving of the model. It was assumed to be normally consolidated or very lightly overconsolidated as it had not experienced a higher stress in its history. Although it is recognised that even loose NC sands may be in a dry-of-critical state, it is possible that the loose sand was initially wet-of-critical and yielded upon engaging the Roscoe Surface early into loading, as hypothesised in Fig. 11a.

In the dense test, the disturbed upper layer resulting in bedding errors would have exhibited some plastic strains prior to the stiffer observed foundation response of the dense, heavily overconsolidated material. At high stresses, after engaging the Hvorslev Surface, plastic strains would be generated as elements strain-softened to critical state, as displayed in Fig. 11c. The generation of plastic strains in this case is obvious, given the observed plastic collapse at ultimate failure.

The most successful prediction was the medium dense sand test. It is hypothesised that the greater accuracy of this prediction was due to strains remaining elastic, as the stress path remained on an elastic wall throughout. Fig. 11b shows the heavily overconsolidated sand (overconsolidated to a considerably lesser degree than the dense test) with a stress path that does not engage the yield curve prior to functional foundation failure. Impractically large deformations would likely be required to engage the yield surface and shear to critical state in this case.

7. Conclusions

A nonlinear stepwise model based on shear modulus degradation behaviour may be used to predict stress-settlement behaviour of strip foundations on dry sand to within 20% of the stresses observed for a physical model for serviceable settlements. Predictions using a modulus reduction curve with rapid initial stiffness degradation resulted in superior predictions.

The predictions for foundations on loose sand ($D_r = 12\%$) and dense sand ($D_r = 90\%$) produced errors of 10.8% and 5.9% at ultimate bearing capacity respectively. The prediction for a foundation on medium dense sand ($D_r = 48\%$) was the most accurate over the full settlement range, as well as at ultimate bearing capacity, where the error was less than 1%. It is proposed that this prediction was most successful due to elastic strains dominating the deformation behaviour in the medium dense model test.

Particle Image Velocimetry (PIV) may be utilised to graphically determine strains throughout loading, and elasticity theory used to determine shear modulus degradation, with satisfactory predictions arising from the back-calculated modulus reduction curves.

A settlement-based failure criterion of 10% of the foundation width was a suitable assumption for tests at all relative densities.

Three different modes of shear failure were achieved across the three tests by varying the initial relative density of the foundation sand, as determined through full-field PIV analyses.

References

American Society for Testing and Materials. 2000. "ASTM Standard D4253: Standard Test Methods for Maximum Index Density and Unit Weight of Soils Using a Vibratory Table." West Conshohocken: ASTM. http://doi.org/10.1520/D4253-00

American Society for Testing and Materials. 2000. "ASTM Standard D4254. Test Methods for Minimum Index Density and Unit Weight of Soils and Calculation of Relative Density." West Conshohocken: ASTM. http://doi.org/10.1520/D4254-00

American Society for Testing and Materials. 2011. "ASTM Standard D2487. Standard Practice for Classification of Soils for Engineering Purposes (Unified Soil Classification System)." West Conshohocken: ASTM. http://doi.org/10.1520/D2487-11

Archer, A. 2014. "Using small-strain stiffness to predict the settlement of shallow foundations on sand." MEng thesis. University of Pretoria. http://doi.org/2263/43358

Archer, A. and Heymann, G. 2015. "Using small-strain stiffness to predict the load-settlement behaviour of shallow foundations on sand." *J. S. Afr. Inst. Civ. Eng.*, 57(2), pp 28-35. http://doi.org/10.17159/2309-8775/2015/v57n2a4

Atkinson, J.H. 1981. "Slopes and Foundations – An introduction to applications of critical state soil mechanics." 1st ed. London: McGraw Hill. ISBN: 9780470272466.

Boussinesq, J.V. 1885. "Applications des potentiels à l'étude de l'équilibre et du mouvement des solides élastiques." (Applications of potentials to the study of equilibrium and motion of elastic solids.) Paris: Gauthier-Villars (in French). http://doi.org/1908/1180

Briaud, J-L. 2007. "Spread Footings in Sand: Load Settlement Curve Approach." *J. Geotech. Geoenviron. Eng.*, 133(8), pp 905-920. http://doi.org/10.1061/(ASCE)1090-0241(2007)133:8(905)

Heymann, G., Rigby-Jones, J. and Milne, C. 2017. "The application of continuous surface wave testing for settlement analysis with reference to a full-scale load test for a bridge at Pont Melin, Wales, UK." *J. S. Afr. Inst. Civ. Eng.*, 59(2), pp 49-58. http://doi.org/10.17159/2309-8775/2017/v59n2a6

Oztoprak, S. and Bolton, M.D. 2013. "Stiffness of sands through a laboratory test database." *Géotechnique*, 63(1), pp 54-70. http://doi.org.10.1680/geot.10.P.078

Stanier, S.A, Blaber, J., Take, W.A. and White, D.J. 2016. "Improved image-based deformation measurement for geotechnical applications." *Can. Geotech. J.*, 53(5), pp 727-739. http://doi.org/10.1139/cgj-2015-0253

Terzaghi, K von. 1943. "Theoretical Soil Mechanics." 1st ed. New York: John Wiley and Sons. http://doi.org/10.1002/9780470172766

Vesić, A.S. 1973. "Analysis of Ultimate Loads of Shallow Foundations." *J. Soil Mech. & Fndn. Div., Proc. ASCE*, 99(1), pp 45-73. http://doi.org/10.1061/JSFEAQ.0001846